Jurnal Teknologi

Full paper

Dynamic Analysis of Flow Field at the End of Combustor Simulator

E. Kianpour[a], Nor Azwadi Che Sidik[a*], Mohsen Agha Seyyed Mirza Bozorg[b]

[a]*Department of Thermo Fluid, Faculty of Mechanical Engineering, UTM, Malaysia*
[b]*Iranian Space Agency (ISA), Tehran, Iran*

*Corresponding author: azwadi@fkm.utm.my

Article history

Received :15 June 2012
Received in revised form :12 August 2012
Accepted :28 August 2012

Graphical abstract

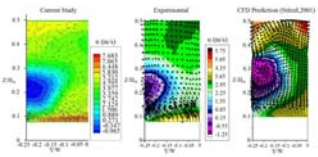

Abstract

This study was carried out in order to extend database knowledge about the flow field characteristics and define the various flow field contours inside a combustor simulator. The modern gas turbine industries try to get higher engine efficiencies. Brayton cycle is a key to achieve this purpose. According to this cycle industries should increase the turbine inlet temperature to get more engine efficiency and power. However the turbine inlet temperature increasing creates an extremely harsh environment for the downstream critical components such as turbine vanes. In this research a three-dimensional representation of a true Pratt and Whitney aero-engine which studied before in Virginia University was simulated and analyzed to collect essential data. This combustor simulator combined the interaction of two rows of dilution jets, which were staggered in the stream wise direction and aligned in the span wise direction, with that of film-cooling along the combustor liner walls. The overall findings of the study indicate that three-component velocity measurements showed the dilution jet-mainstream interaction produced shear forces and as a result a counter-rotating vortex pair was created. The highest turbulent kinetic energy was found at the top of recirculating region due to the interaction of the second row of dilution jets and mainstream flow. Furthermore, the centers of the counter-rotating vortex pair were spread relatively far apart due to the opposing dilution jets. Along the dilution jet centerline, negative stream wise velocities were measured indicating the recirculation region just downstream of the jet. Into the combustor exit, the acceleration of the flow increased and thereby the uniformity of the velocity profile enhancement was found as well.

Keywords: Flow fields, gas turbines, dilution holes, film-cooling, cooling holes

1.0 INTRODUCTION

The modern gas turbine industries try to construct new engines with higher efficiencies. Brayton cycle is a key to afford this purpose. As seen from this cycle, the turbine inlet temperature should increase to access more efficiency. Nevertheless the turbine inlet temperature increasing creates an extremely harsh environment for the downstream components. Fuel must be thoroughly mixed with air, completely burned and made uniform before turbine. However poor mixing leads to non-uniformities such as hot streaks and allow non-combusted fuel to exit the combustor. Hot streaks can harm wear prematurely and failure turbine components. According to the importance of this research, a broad literature search was conducted to collect the information and specify the combustor characteristics.

Harrington, McWaters, Bogard, Lemmon and Thole [i] presented a study which was a computational and experimental one aiming at investigating a full coverage of adiabatic film cooling effectiveness. The results declare that maximum adiabatic film cooling effectiveness is achieved within four to eight rows of cooling holes.

Barringer, Richard, Walter, Stitzel and Thole [ii] studied the flow field at the inlet of turbine vanes. This test section contained four different cooling panels. Two rows of high momentum dilution jets were designed in the second and third cooling panels. They confirmed the Li, Liu and Peng [iii] and Scrittore [iv] results that how dilution jets affect cooling.

By using the multiple jets placed inside cross flow, Peterson and Plesniak [v] analysed the effects of velocity, blowing ratio, injection angle and the plenum flow direction. Consistent with the study of Plesniak [vi], the results declare that a light and less integrated CRVP is created due to the vortices spawn inside injection hole and opposite rotation direction which is opposite the rotational sense of the CRVP by using the counter-flow plenum.

The results indicate that the usage of air and carbon dioxide as a coolant influence the effects of blowing ratio on the heat transfer coefficient and also it is in consistent with Mehendale, Han, Ou and Lee [vii,viii]. For carbon dioxide, heat transfer coefficient is increased at first and then decreased with blowing ratio enhancement, while for the air injection, heat transfer coefficient has fluctuations. In addition, the density ratio affected the distributions of the streamwise heat transfer coefficient significantly.

Tarchi, Facchini, Maiuolo and Coutandin [ix] were able to identify the effects of large dilution hole which place within penetrating slot and effusion array. In this study, the local heat transfer coefficient and adiabatic film cooling effectiveness were

measured at three different blowing ratios. In concurred with Tarchi, Facchini, Maiuolo and Coutandin [x] and Milanes, Kirk, Fidkowski and Waitz [xi], it is found that with using backward step, at downstream the dilution hole the adiabatic film cooling effectiveness reached to η_{aw}=0.65.

Baldauf, Schulz and Wittig [xii] determined test results of coolant injected from cylindrical holes with d=5mm. In particular, blowing angle, hole pitch, blowing rate and density ratio variations were investigated. Experimental results show that the heat transfer coefficient extremely away from the situation without coolant ejection is highly relating to the blowing situation. Heat transfer coefficient increased by 120% over the great downstream distances compared to unblown baseline case.

Scrittore, Thole and Burd [xiii] measured the flow characteristics inside a combustor simulator. For uncertainty analysis, they used Moffat [xiv] partial derivative and sequential perturbation methods. The results showed that the penetration height of coolant is not dependent to the mass blowing ratios, at least among the specific range. Like previous studies as Bernsdorf, Rose and Abhari [xv], film cooling effectiveness enhancement for the film layer occurred with blowing ratios, especially at high blowing ratios.

Using a two dimensional particle image velocimetry, Wright, McClain and Clemenson [xvi] measured the effects of cooling jet turbulence intensities and blowing ratios of cylindrical and simple angle holes. The results indicate that for both turbulent intensities, flow attached to the surface at lowest blowing ratio of 0.5. Also, Tehrani and Mahmoodi [xvii] stated that at blowing ratio of M=0.50 and inclination angle of 35deg, the film cooling effectiveness reached to the optimum value. The horse shoe vortex and counter rotating vortices were formed around jets as well.

Stitzel and Thole [xviii] indicated that dilution jet injection is dominant feature at the combustor exit, while, with no dilution, the exit profile was relatively uniform with a high temperature and low total pressure flow in the mainstream. Furthermore Scrittore [xix] mentioned that dilution jet velocity increase has adverse effect on surface cooling performance downstream of dilution jets.

According to the importance of issue, the cooling of combustor exit flow requires further study and numerical analyses. There are questions to be answered: What is the effect of changing the cooling holes area on combustor exit profiles? What is the effect of cooling holes configuration variations on exit flow?

This numerical study was done in order to optimize the combustor exit and cooling holes geometries. In this study, the effects of various combustor holes geometries were analysed as well. Also in order to measure the validity of the results, a comparison between the data gained from this study and Vakil and Thole [xx] project was made.

2.0 METHODS AND MATERIALS

In this study, a three-dimensional representation of a true Pratt and Whitney aero-engine was simulated and analysed to gain essential data. The combustor is a container with a width and height of 111.8cm and 99.1cm respectively. The length of the combustor was 156.9 cm and the contraction angle was 15.8 degrees. While the inlet cross-sectional area was 1.11 square meter, the exit cross-sectional area was 0.62 square meter. The contraction angle began at X=79.8 cm. The combustor simulator included a stream wise series of four film-cooled panels. The starting point of these panels was approximately at 1.6 m upstream of the turbine vanes. The lengths of the first two panels are 39cm and 41 cm respectively. However the third and fourth panels are 37 and 43 centimetre in length. The panels were 1.27 cm in thick. At the result of using the material with low thermal conductivity (k = 0.037 W/mk), adiabatic surface temperature measurements were possible. Within the second and third panels were two rows of dilution holes. The first row was embedded at 0.67 m downstream of the beginning of the combustor liner panels. The diameter of the first row and second row of dilution holes was 8.5 cm and 11.9 cm respectively. The first row was located at 0.90 m downstream of the start of the combustor simulator. The centreline of the second row was staggered with respect to those of the first row. To verify the purpose of this study, a three-dimensional representation of a true Pratt and Whitney aero-engine which studied before in Virginia University was simulated [20], however, the combustor with various configurations of cooling holes, were simulated. While, the first arrangement was similar to the Vakil and Thole [20] model, the second case was completely different. The film-cooling holes were placed in equilateral triangles. The film-cooling holes diameter of the first model (Case 1) was 0.76 cm and drilled at an angle of 30 degrees from the horizontal surface. The length of each film-cooling hole was 2.5 cm. The film-cooling holes of the second combustor simulator (Case 2) were 1.70 cm in diameter and drilled at an angle of 30 degrees from the horizontal surface. Figures 1a (Case 1) and 1b (Case 2) show the schematic view of the combustor simulator. To have a similar criterion between both arrangements, a global coordinate system (X, Y, and Z) was selected.

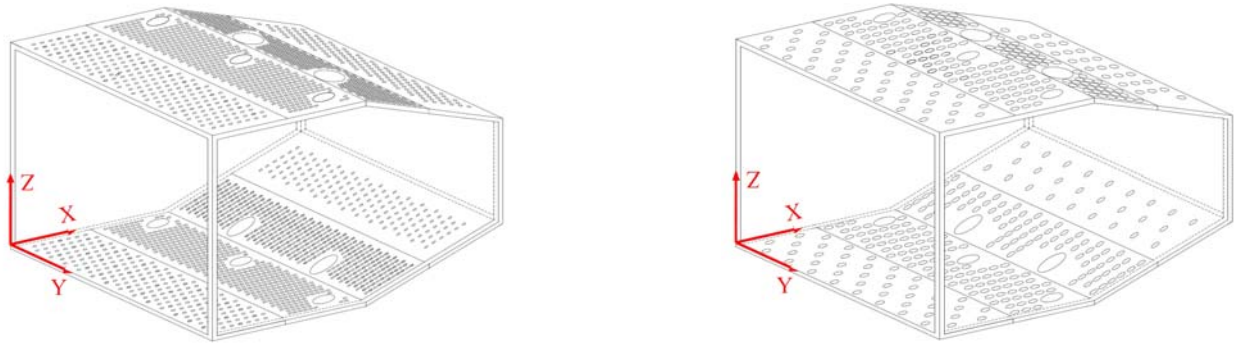

(a) (b)

Figure 1 Schematic view of the combustor simulator (a) Case 1 (b) Case 2

The flow field measurement planes in the combustor simulator illustrated in Figure 2a (Case 1) and 2b (Case 2). Plane 0p, was placed exactly downstream of the first panel of cooling holes to determine the momentum distribution of film cooling along the mentioned panel. Plane 1p covered half of the combustor simulator was selected to capture the horseshoe, half-wake, and counter-rotating vortex.

Plane 2p was intended to show the interaction of the counter-rotating vortex pairs from the first and the second dilution. Plane 3p was intended to show the flow field behaviour at the end of combustor and inlet of turbine. Plane 1s was selected at Y=22.83 cm and would depict the lip, half-wake, or half-wall vortices.

In order to solve the combustor simulator and to get more correct data and reasonable time consumption, about 1×10^6 tetrahedral meshes were required. The accuracy of the quantity of meshes which used in this study was in concurred with Stitzel and Thole investigation [18]. As seen in these figures, the meshes were denser around the cooling and dilution jets as well as wall surfaces (Figure 3).

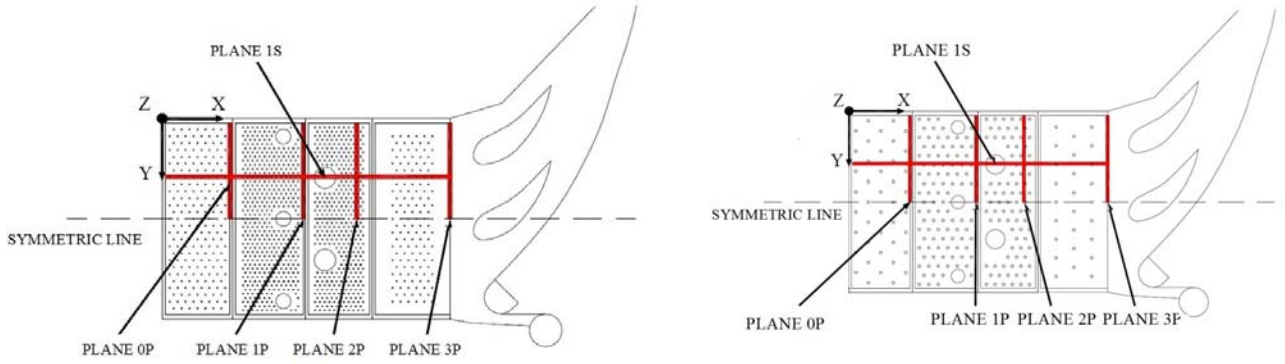

Figure 2 Location of the measured planes (a) Case 1 (b) Case 2

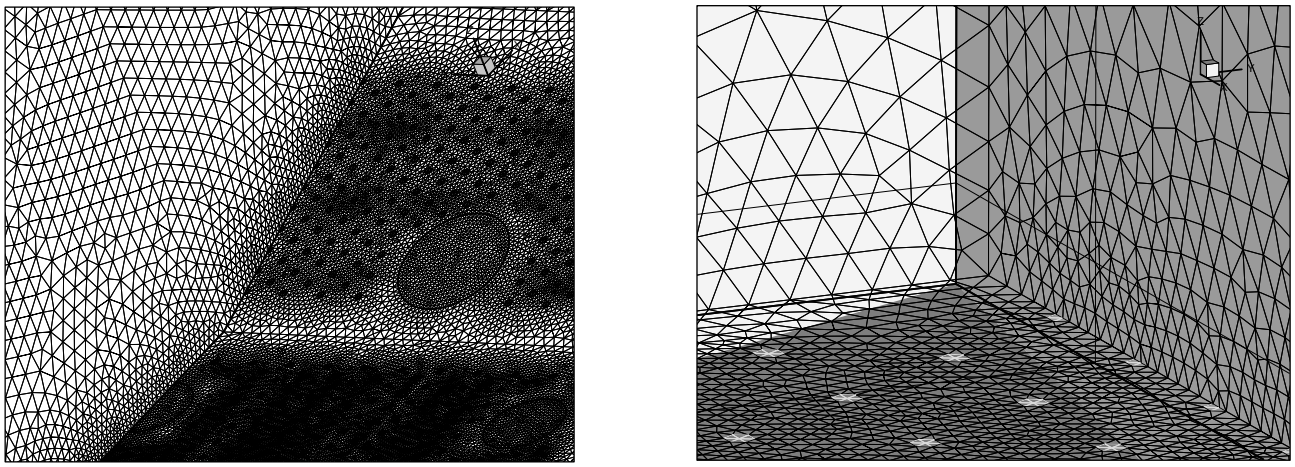

Figure 3 Three-dimensional meshes of combustor simulator (a) Case 1 (b) Case 2

According to the specific flow rate at the inlet of volume control, inlet mass flow boundary layer was defined at the inlet. Wall boundary layer and slip less boundary layer were applied to limit the interaction zone between fluid and solid layer. Furthermore at the inlet of combustion simulator the uniform flow boundary layer was selected. Also at the end of volume control the constant pressure boundary layer was used. Finally, according to the symmetries of the Pratt and Whitney aero-engine combustor along X-Y and X-Z planes, symmetry boundary layer $\frac{\partial}{\partial \mathrm{n}}=0$ was applied. In addition the governing equations were used.

Continuity equation

$$\frac{\partial \rho}{\partial t}+\frac{\partial}{\partial x}\frac{dx}{dt}+\frac{\partial \rho}{\partial y}\frac{dy}{dt}+\frac{\partial \rho}{\partial z}\frac{dz}{dt}=-\rho\left(\nabla.V\right) \quad (1)$$

Momentum equation

$$\frac{\partial}{\partial t}\left(\rho u_i\right)+\frac{\partial}{\partial x_j}=\left(\rho u_i u_j\right)=-\frac{\partial P}{\partial x_i}+\frac{\partial \tau_{ij}}{\partial x_i}+\rho g_i+\vec{F}_i \quad (2)$$

Energy equation

$$\frac{\partial}{\partial t}\left(\rho E\right)+\frac{\partial}{\partial x_i}\left(u_i\left(\rho E+P\right)\right)=\frac{\partial}{\partial x_i}\left(K_{eff}\frac{\partial T}{\partial x_i}-\sum_{j'}h_{j'}J_{j'}+u_j\left(\tau_{ij}\right)_{eff}\right)+S_h \quad (3)$$

and K- equation

$$\frac{\partial}{\partial t}\left(\rho k\right)+\frac{\partial}{\partial x_i}\left(\rho k u_i\right)=\frac{\partial}{\partial x_j}\left[\left(\mu+\frac{\mu_t}{\sigma_k}\right)\frac{\partial k}{\partial x_j}\right]+P_k+P_b-\rho\varepsilon-Y_M+S_k \quad (4)$$

$$\frac{\partial}{\partial t}(\rho\varepsilon)+\frac{\partial}{\partial x_i}(\rho\varepsilon u_i)=\frac{\partial}{\partial x_j}\left[\left(\mu+\frac{\mu_t}{\sigma_\varepsilon}\right)\frac{\partial\varepsilon}{\partial x_j}\right]+C_{1\varepsilon}\frac{\varepsilon}{k}(P_k+C_{3\varepsilon}P_b)-C_{2\varepsilon}\rho\frac{\varepsilon^2}{k}+S_\varepsilon \quad (5)$$

The difference between the last results with new data is defined by converge magnitude and this measure reduction means access to the more exact data. According to the iteration chart of solution, converge quantity of this solution was about 10^{-3}. Also to solve this question, unsteady condition was applied. This condition led to different iterations. While large iteration shows the time step variations and beginning the new step, small variations were completely related to the physics of the question and they continued to get the new time step. The combustor simulator was meshed by Gambit software and the collected data were analysed by using fluent software and the corresponding results were presented in the form of charts and different contours. Although there were several ways to investigate the validation of the numerical findings, the best way to valid the results of this study was comparing the results with those of other related studies. This method was too cheaper and easier compared to other methods such as experimental tests and computational programming, while the results were not more reliable.

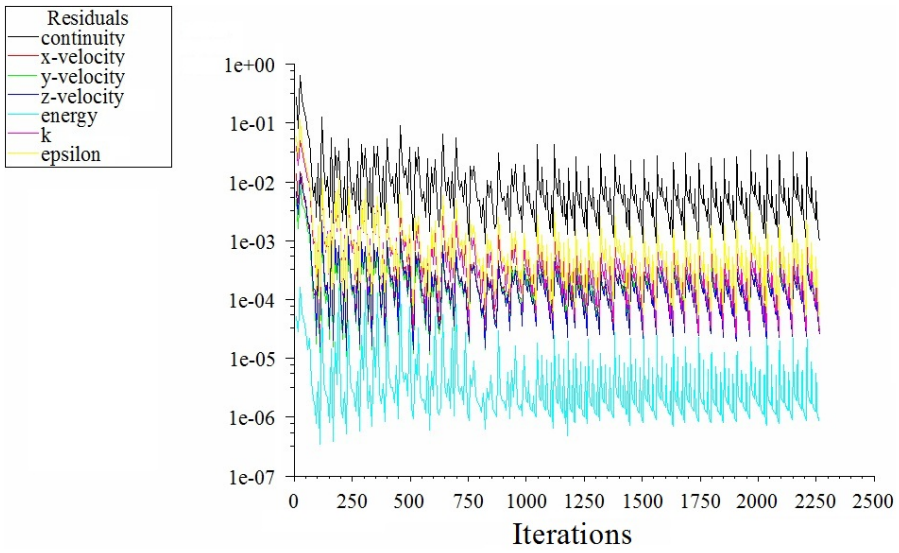

Figure 4 The remnant chart of the solution of this problem

■3.0 RESULTS AND DISCUSSION

Figures 4a and 4b show the three-component velocity measurements of plane 1p for both arrangements. This measurement plane included one entire pitch with one dilution jet centred at Y=12cm and the other at Y=48cm. The counter-rotating vortex of the middle dilution jet pair, seen in detail was the distinctive part of these figures. The shear produced due to the dilution jet-mainstream interaction led to these vortexes. In addition, due to the impacts between the opposing rows of dilution jets, the centres of the counter rotating vortex pair spread further far. The size of the counter-rotating vortex pair was quite large. Also these vortexes extended over most of the vertical cross-sectional area within the measurement plane.

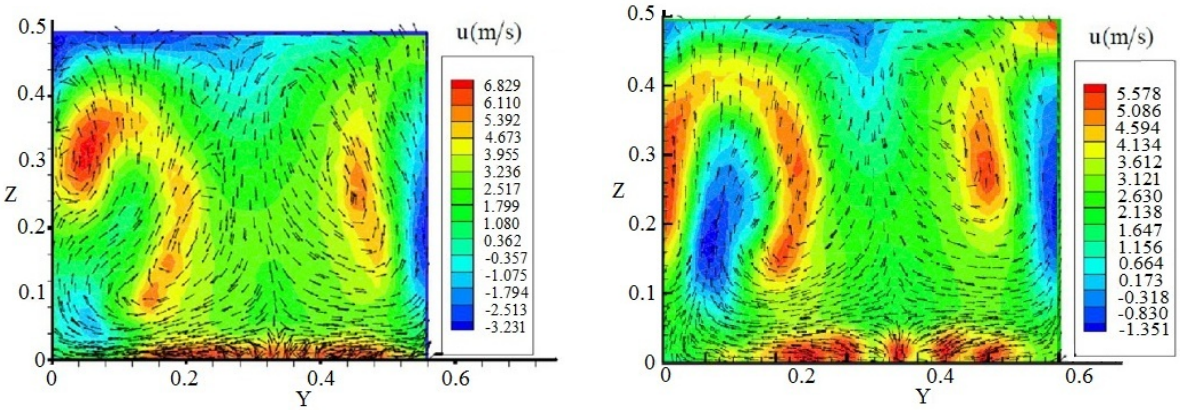

(a) (b)

Figure 4 Three-component velocity of plane 1p (a) Case 1 (b) Case 2

Figures 5a and 5b indicate the contour plots of the combustor turbulent kinetic energy in plane 1p for two different configurations. As it can be seen from this chart, the highest turbulent kinetic energies were found slightly to the right side of the centre of the counter-rotating vortex. In this area, the impacts between the two opposed dilution jets caused to the lowest stream wise velocity components. In general, for the first configuration, the highest magnitude of turbulent kinetic energy was found near the centre of the counter-rotating vortex and among the impact region.

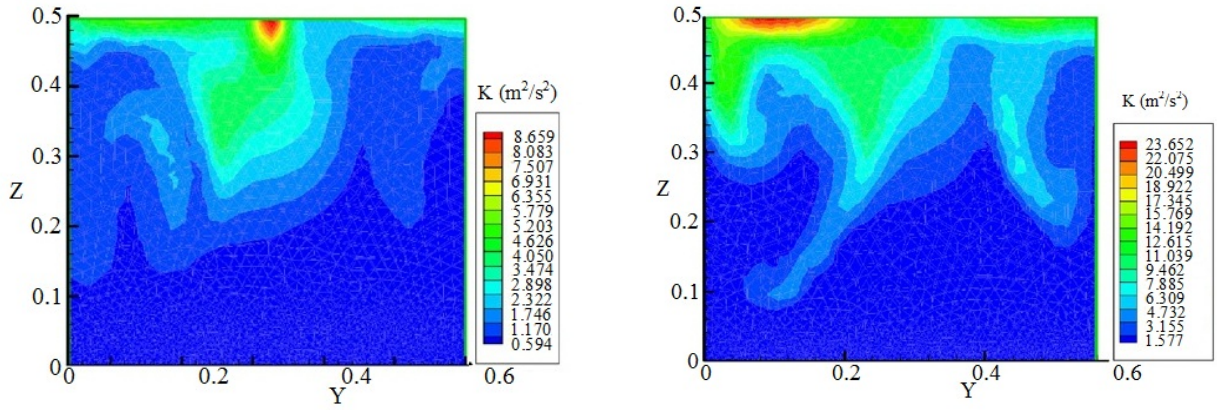

(a) (b)

Figure 5 Contours of the combustor turbulent kinetic energy for plane 1p (a) Case 1 (b) Case 2

Figures 6a and 6b declare the vectors of u and w for plane 1s. Between 84cm ≤ X ≤ 94cm the ejection of flow among the dilution hole was obvious. In addition at Z=30 cm the core of the dilution jet began to deflect sharply by the combustor mainstream. At the leading edge, the flow was angled downward due to the impacts of the dilution jets. The most important reason for this behaviour was the deflection of the flow under the stagnation region created at the midspan by the first row of dilution jets. In a word, with the flow acceleration, the uniformity of the velocity profiles increased towards the combustor exit. However, at the combustor exit, traces of the faster film-cooling and midspan regions were still visible in the streamwise velocity profiles.

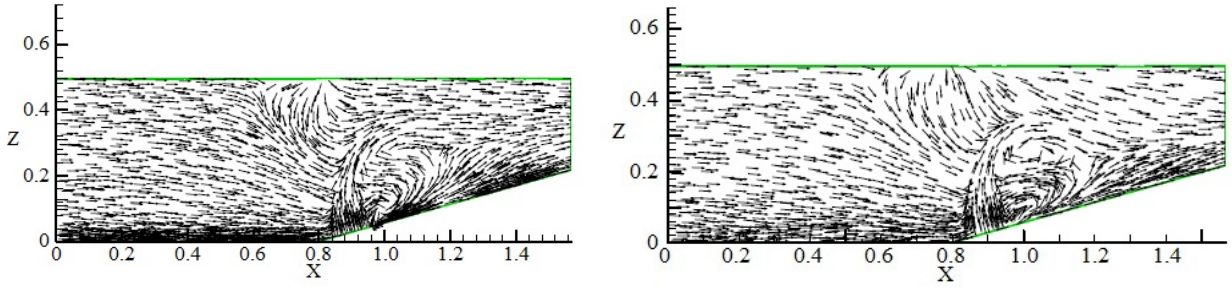

(a) (b)

Figure 6 Vectors of u and w for plane 1s (a) Case 1 (b) Case 2

Figures 7a and 7b present the three-component velocity measurements of plane 2p for both cases of cooling holes schemes. The most immediate feature of figures 6 was the recirculating region behind the dilution jet. At Z=24.8 cm, small negative streamwise velocities were visible. The v and w vectors determine a leftward sweeping motion along the film-cooling panel. The stream wise non-uniform velocity components state the non-uniformities at the end of combustor profile.

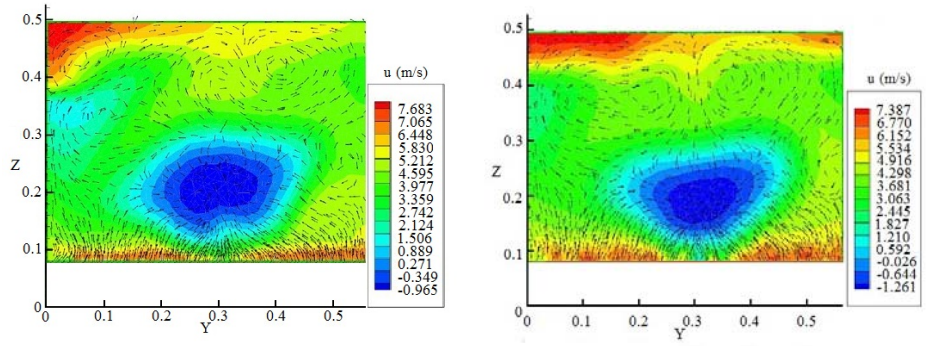

(a) (b)

Figure 7 Three-component velocity for plane 2p (a) Case 1 (b) Case 2

Figures 8a and 8b indicates the contours of the combustor turbulent kinetic energy for plane 2p. The largest values of turbulent kinetic energies were present at the top of the recirculating region. However, the shear forces in this turning region produced the highest turbulence among the flow.

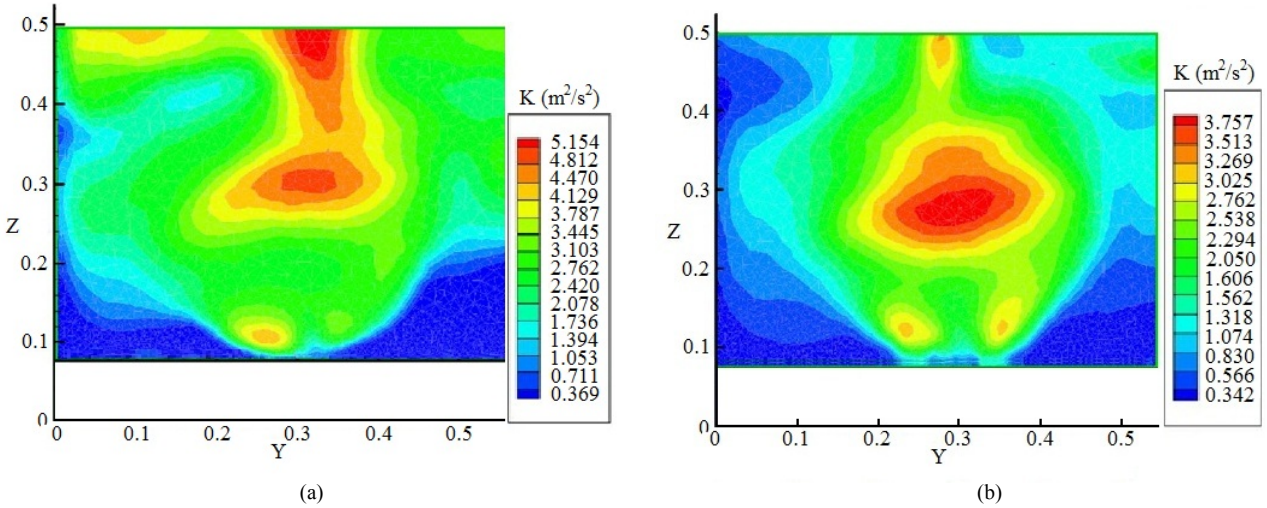

(a) (b)

Figure 8 contours of turbulent kinetic energy in plane 2p (a) Case 1 (b) Case 2

Figure 9 shows the streamwise velocity components at the end of combustor. According to this figure, the counter-rotating vortex increased with passing the time. This counter-rotating vortex created because of the shear produced due to the first and second row of dilution jet and mainstream interaction.

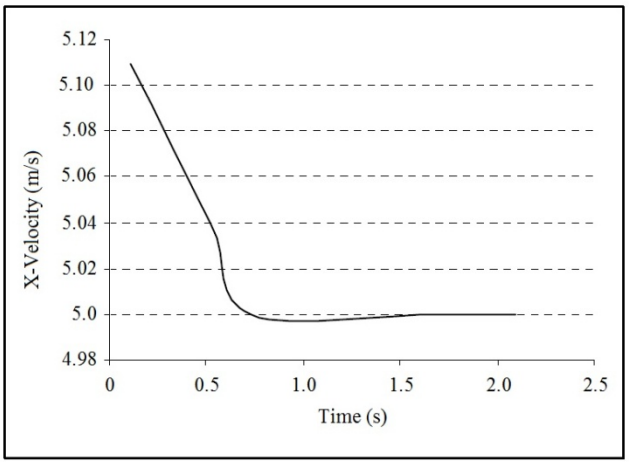

Figure 9 the variations of streamwise velocity per time for plane 3p

Figures 10a and 10b show the contours of the streamwise velocities which solved by the RNGK-ε and K-ε turbulent models. As it can be seen from these contours, the RNGK-ε turbulent model prepared more uniform turbulence distribution compared to turbulence kinetic energy contour obtained by using K-ε turbulent model.

Figure 11 shows a comparison of the velocity contours and v and w vectors measured experimentally and computationally. According to the computational results, the dilution jet injection led to flow entrainment near the surface. As a result, the entrainment of the flow to the left side was similar between experimental observations and computational findings. The existence of three primary vortices in computational results was the clear difference between computational and experimental data. These vortices were the remnants of the first row of dilution jets with the mainstream and second row of dilution jets interaction.

Figure 12 shows that the uncertainty between computational outputs and experimental results for plane 2p was about 8 percent.

4.0 CONCLUSION AND RECOMMENDATION

The purposes of this study were extending the database knowledge about the flow field characteristics inside a combustor simulator and define the effects of number of cooling holes and area variation on floe field. In this research a three-dimensional presentation of a true Pratt and Whitney aero-engine was simulated and analyzed to collect data. The combustor was meshed by Gambit software and the collected data were simulated and analyzed by using fluent software and the corresponding results were presented in the form of charts and different contours. To sum up, the film-cooling jets nearest to the last row of measurement plane had their coolest region on

the wall. Also, these jets made a secondary cool region slightly further off the wall. This secondary region was a remnant of the upstream row of film-cooling jets that exited from an aligned cooling hole. The shear which produced from the dilution jet-mainstream interaction led to a counter-rotating vortex pair. The centres of the counter-rotating vortex pair were spread relatively far apart due to the opposing dilution jets. Along the dilution jet centreline, the existence of negative stream wise velocities indicate the recirculating region just downstream of the jet. Comparisons between experimental and computational results indicate similarities, as well as differences. The entrainment of the flow to the left side was similar between experimental observations and computational data. Despite this similarity, the existence of three primary vortices in computational results was the clear difference between computational and experimental data. In the future research, additional flow field measurements should be considered at the leading edge of the dilution jets. This consideration could be useful to document the presence and effects of a horse-shoe vortex. It is highly recommended that the future research study the different cooling holes shapes. Different cooling holes shapes affect the interaction between the cooling flow and main flow.

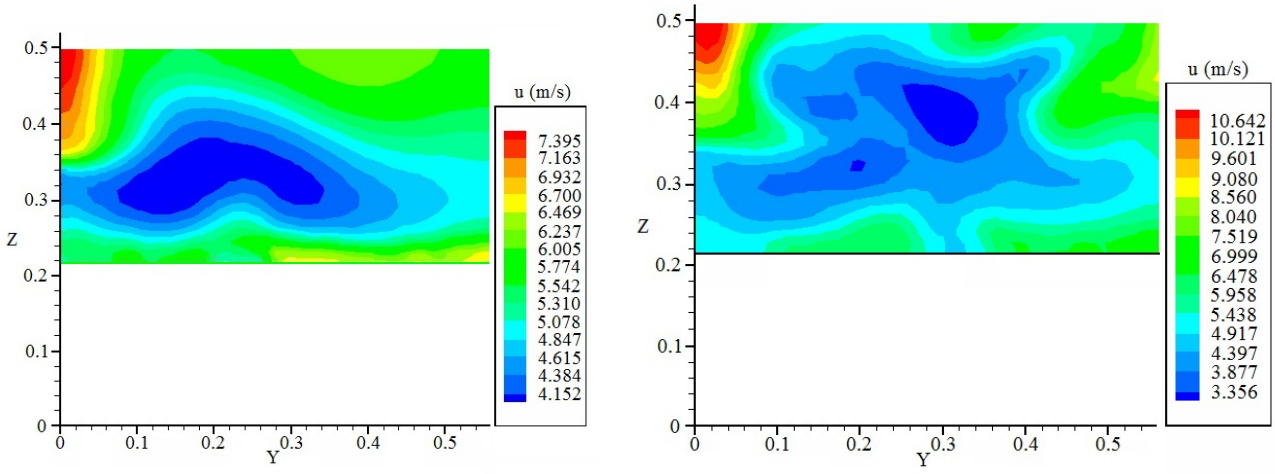

(a) (b)

Figure 9 Contours of the stream wise velocities (a) K-□ turbulent model (b) RNGK-□ turbulent model

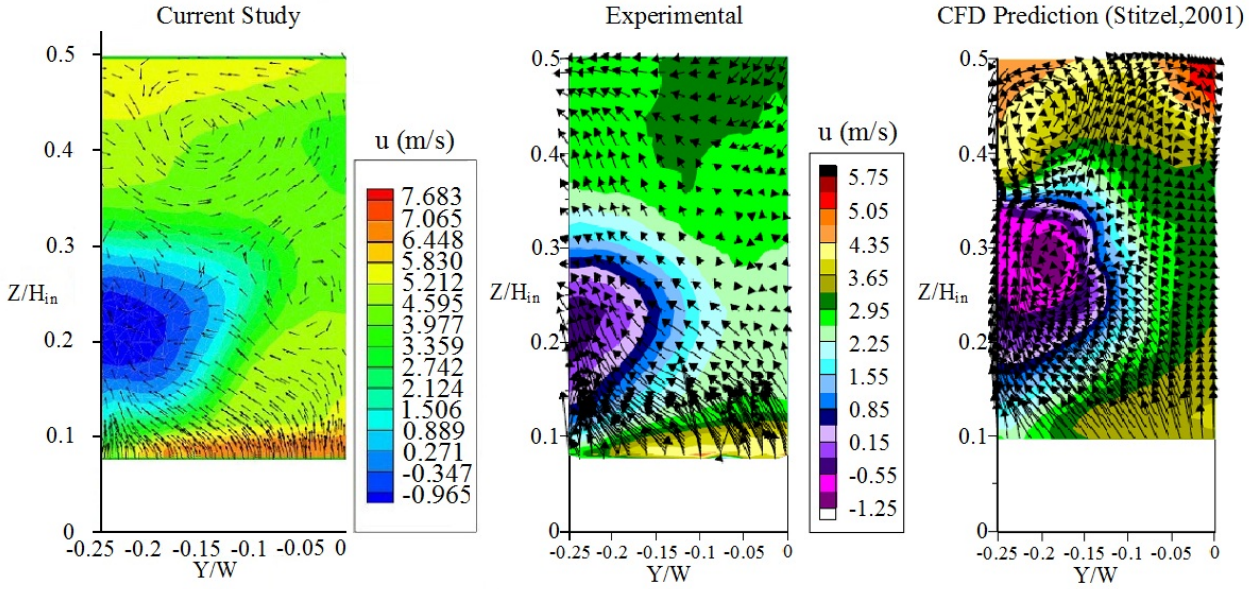

Figure 10 Comparison of u contours and v and w vectors for plane 2p

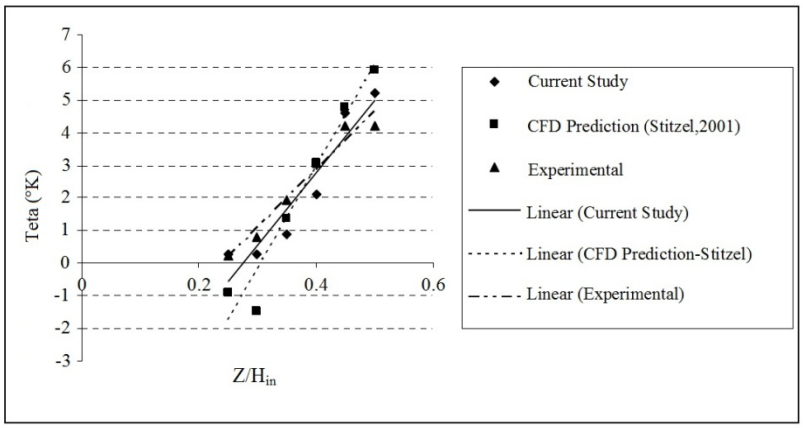

Figure 11 Uncertainty analysis for plane 2p at $Z/H_{in} = 0.27$

References

[1] Harrington, M. K., & McWaters, M. A., & Bogard, D. G., & Lemmon, C. A., & Thole K. A. 2001. Full-Coverage Film Cooling With Short Normal Injection Holes. *Journal of Turbomachinery*. 123: 798–805.

[2] Barringer, M. D., & Richard, O. T., & Walter, J. P., & Stitzel, S. M., & Thole, K. A. 2002. Flow Field Simulations of a Gas Turbine Combustor. *Journal of Turbomachinery.* 124: 508–516.

[3] Li, L. & Liu, T. & Peng, X. F. 2005. Flow Characteristics in an Annular Burner with Fully Film Cooling. *Journal of Applied Thermal Engineering.* 25: 3013–3024.

[4] Scrittore, J. J. 2008. Experimental Study of the Effect of Dilution Jets on Film Cooling Flow in a Gas Turbine Combustor. PhD theses. Virginia Polytechnic Institute and State University, Virginia. 160.

[5] Peterson, S. D., & Plesniak, M. W. 2002. Short-hole Jet-in-cross Flow Velocity Field and Its Relationship to Film-cooling Performance. *Experiments in Fluids*. 33: 889–898.

[6] Plesniak, M. W. 2006. Noncanonical Short Hole Jets-in-Crossflow for Turbine Film Cooling. *Journal of Applied Mechanics.* 73: 474–482.

[7] Ou, S., & Je-Chin, H., & Mehendale, A. B., & Lee, C. P. 1994. Unsteady Wake Over a Linear Turbine Blade Cascade with Air and CO2 Film Injection: Part I—Effect on Heat Transfer Coefficients. *Journal of Turbomachinery*. 116: 721–729.

[8] Mehendale, A. B., & Je-Chin. H., & Ou, S., & Lee, C. P. 1994. Unsteady Wake Over a Linear Turbine Blade Cascade with Air and CO2 Film Injection: Part II—Effect on Film Effectiveness and Heat Transfer Distributions. *Journal of Turbomachinery*. 116: 730–737.

[9] Tarchi, L., & Facchini, B., & Maiuolo, F., & Coutandin, D. 2012. Experimental Investigation on the Effects of a Large Recirculating Area on the Performance of an Effusion Cooled Combustor Liner. *Journal of Engineering for Gas Turbines and Power*. 134:. 041505-1-041505-9.

[10] Tarchi, L., & Facchini, B., & Maiuolo, F., & Coutandin, D. 2012. Experimental Investigation on the Effects of a Large Recirculating Area on the Performance of an Effusion Cooled Combustor Liner. *Journal of Engineering for Gas Turbines and Power.* 134: 041505-1-041505-9.

[11] Milanes, D. W., & Kirk, D. R., & Fidkowski, K. J., & Waitz, I. A. 2006. Gas Turbine Engine Durability Impacts of High Fuel-Air Ratio Combustors: Near Wall Reaction Effects on Film-Cooled Backward-Facing Step Heat Transfer. *Journal of Engineering for Gas Turbines and Power.* 128: 318–325.

[12] Baldauf, S., & Schulz, A., & Wittig, S. 2001. High-Resolution Measurements of Local Heat Transfer Coefficients from Discrete Hole Film Cooling. *Journal of Turbomachinery.* 123: 749–757.

[13] Scrittore, J. J., & Thole, K. A., & Burd, S. W. 2007. Investigation of Velocity Profiles for Effusion Cooling of a Combustor Liner. *Journal of Turbomachinery.* 129: 518–526.

[14] Moffat, J. R. 1988. Describing the Uncertainties in Experimental Results. *Exp. Therm. Fluid Sci.* 1: 3–17.

[15] Bernsdorf, S., & Rose, M., & Abhari, R. S. 2006. Modeling of Film Cooling—Part I: Experimental Study of Flow Structure. *Journal of Turbomachinery.* 128: 141–149.

[16] Wright, L. M., & McClain, S. T., & Clemenson, M. D. 2011. Effect of Freestream Turbulence Intensity on Film Cooling Jet Structure and Surface Effectiveness Using PIV and PSP. *Journal of Turbomachinery.* 133: 041023-1- 041023-12.

[17] Bazdidi Tehrani, F., & Mahmoodi A. *A. Finite Element Analysis of Flow Field in the Single Hole Film Cooling Technique*. Annals New York Academy of Science. 393–400.

[18] Stitzel, S., & Thole, K. A. 2004. Flow Field Computations of Combustor-Turbine Interactions Relevant to a Gas Turbine Engine. *Journal of Turbomachinery.* 126: 122–129.

[19] Scrittore, J. J. 2008. Experimental Study of the Effect of Dilution Jets on Film Cooling Flow in a Gas Turbine Combustor. PhD theses. Virginia Polytechnic Institute and State University, Virginia. 160.

[20] Vakil, S. S., & Thole, K. A. 2005. Flow and Thermal Field Measurements in a Combustor Simulator Relevant to a Gas Turbine Aero engine. *Journal of Engineering for Gas Turbines and Power.* 127: 257–267.